Development of an enduro mountain bike using purely metallic materials in combination with modern computational and manufacturing methods

Luca Bühlmann[a]

[a] *FHNW - University of Applied Sciences Northwestern Switzerland, Klosterzelgstrasse 2, Windisch, 5210, , Switzerland*

Abstract

The aim of the work was to develop an enduro bike made from purely metallic materials using modern computational and manufacturing methods to provide a high-quality alternative to the competitors made from CFRP. The CO_2-equivalent of manufacturing a steel frame is three to four times lower compared to a carbon frame [9, p. 343]. In addition, at the end of the product life there are no industrial possibilities for recycling of CFRP that are not associated to down-cycling [5]. The engineering work included the evaluation of a geometry, the development of kinematics ideally suited to the overall concept and the subsequent design and dimensioning of the frame structure. By applying topology optimization and additive manufacturing, optimal material efficiency could be achieved. The construction is based on the EFBE test program of category 5, which includes cyclic and static loads. Various joining processes consisting of brazed and welded joints were tested and characterized to ensure mechanical strength. The desired concept was implemented by using butted steel tubes for the main trianlge, which are connected with topology-optimized, 3D-printed lugs from 17-4 PH steel. The swing arm was realized as a lightweight milled component made from a EN AW-2099 T83 high-strength aluminium-lithium alloy.

Keywords: suspension development, topology optimization, joining of SLM printed components, finite element simulation

1. Introduction

In recent years, the popularity of enduro mountain biking has surged, attracting riders with its blend of fast downhill descents and challenging uphill climbs. While the market offers a range of carbon fiber frames, Lean Cycles seeks to innovate by developing an enduro bike made entirely from metallic materials. This paper outlines the collaborative effort between Lean Cycles and FHNW to design and manufacture such a bike, emphasizing the advantages of metallic materials over carbon fiber. By leveraging modern computational and manufacturing methods, the goal is to create a high-performance, sustainable alternative for the mountain biking community.

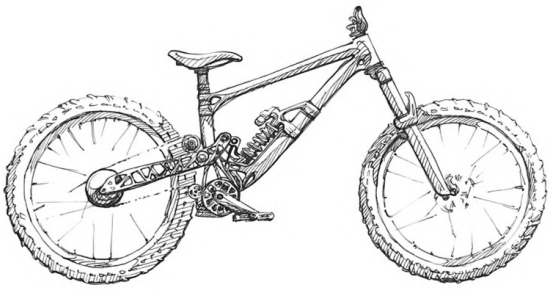

Figure 1: Concept

The choice of materials for the main frame and swingarm is a central aspect in bicycle design. While contemporary bicycle manufacturers often utilize carbon fiber reinforced polymer (CFRP) as frame material due to its high mechanical properties and suitability for applications requiring high stiffness and low weight [7, p. 272], it comes with certain drawbacks. CFRP components are susceptible to damage from impacts during technical enduro downhill rides, leading to delamination or cracking, which can be hardly detected and compromises their structural integrity [8, p. 62]. Additionally, CFRP frames have a significantly higher environmental impact in terms of energy consumption during manufacturing [9, p. 343] and there are no effective recycling methods at the end of their lifecycle [5]. To address these concerns, a shift towards materials with high impact resistance and recyclability is warranted. In this context, the concept for the bike frame presented herein focuses on utilizing steel for the main tubes due to its high toughness [6, p. 405] and ductility [1, p. 122], providing enhanced damage tolerance and better environmental sustainability [10] & [2, p. 30]. Furthermore, the integration of 3D-printed lugs enables the reduction of manual fabrication efforts and offers geometric flexibility, while optimizing material usage and allowing customization according to customer preferences. These design considerations underscore the commitment to developing a high-performance, environmentally conscious enduro mountain bike.

2. Materials and Methods

2.1. Frame Geometry

The determination of the frame geometry was carried out through a systematic process. Initially, the relevant geometric elements and their influences were evaluated. Subsequently,

a comparative analysis was conducted using a rating table to assess the various frame geometries and their associated riding characteristics. A total of five enduro bikes underwent test rides, followed by evaluations based on the gathered impressions by two experienced riders. The geometry of the Lean Cycles prototype was established based on these experiences.

2.2. Kinematics

The design of mountain bike suspensions is a key focus for both industry and research. Previous studies, have explored dynamic models to address issues like pedal-induced bobbing [3]. Despite the significant effort involved, these analyses only consider a single ideal scenario and focus on a fixed set of parameters related to slope, saddle height, and pedaling cadence. However, dynamic models are complex and require extensive calibration, making them less practical. Therefore, this study adopts a quasi-static design approach, which is widely used in practice and offers practical effectiveness despite its simplifications. This includes the assessment of anti-squat and anti-rise values, formulated under quasi-static conditions. Additionally, it involves the impact of the wheel path and the consequent pedal kickback. Lastly, the transmission ratio from the rear suspension to the damper element is outlined, playing a crucial role in determining suspension behavior.

The squat effect describes the compression and extension of the rear suspension due to acceleration during pedaling. This rocking motion is caused by a torque around the pivot of the kinematics. Since the system is in equilibrium before acceleration, the static components of the weight force can be disregarded [4, p. 176]. At 100% anti-squat, the chain force counters mass transfer, achieving equilibrium in resulting moments, what avoids squat effects.

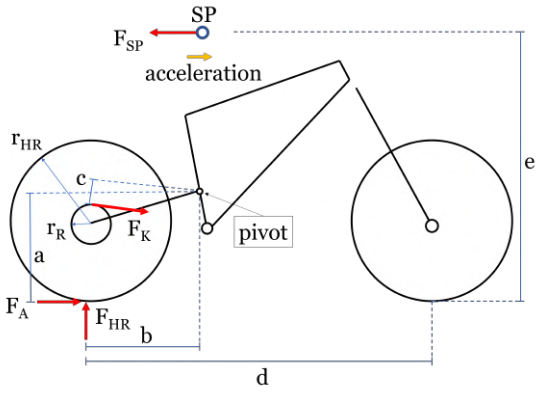

Figure 2: Anti-Squat

$$Anti - Squat = \frac{100\% \times (a + c \cdot \frac{r_{HR}}{r_R})}{b \cdot e_d} \quad (1)$$

The anti-rise value concerns the forces that occur at the rear wheel during braking and their effects on the suspension. Similar to the anti-squat calculation, only the dynamic components resulting from the braking process are considered here. The figure 3 illustrates the forces involved in the anti-rise calculation [4, p. 170]. If the braking torque matches the wheel load torque (100 % anti-rise), the spring-damper element remains neutral, neither compressing nor extending.

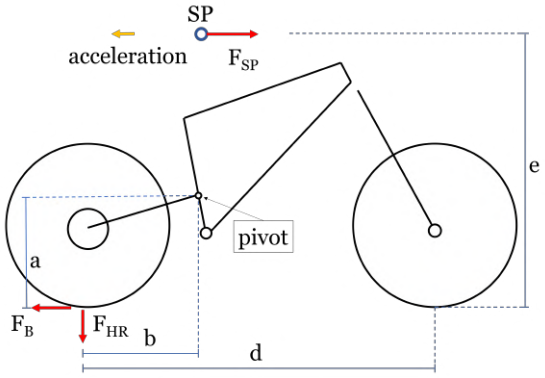

Figure 3: Anti-Rise

$$Anti - Rise = 100\% \times \frac{a}{\frac{e}{d} \times b} \quad (2)$$

When the rear wheel encounters an obstacle, it experiences a force pointing in a specific direction, represented by force vector F. This force can be decomposed into tangential and radial components. Higher tangential components are reached by a high pivot and can be associated with improved responsiveness of the suspension.

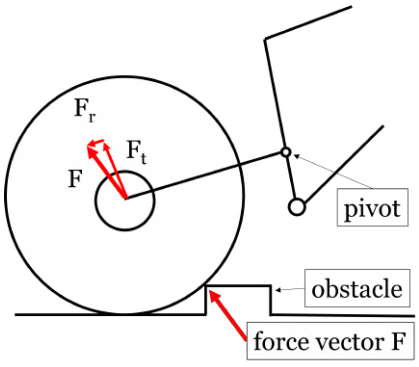

Figure 4: Wheel Path

A higher pivot point in suspension kinematics enhances responsiveness but also leads to pedal kickback, where the crank rotates opposite to pedaling during significant compression. This occurs due to differing elevation curves between the rear wheel hub and the chain. As the rear suspension compresses, it induces chain elongation, requiring a crank rotation to compensate, the so called pedal kickback (see figure 5).

The leverage ratio is determined by the ratio of rear wheel travel to damper stroke. A high ratio requires less force for compression, while a low ratio demands more force. Kinematics dictate the Leverage Ratio and can be modified through design. Enduro mountain bikes require progressive rear suspensions. Progressive behavior entails a higher leverage ratio initially to absorb small obstacles effectively and a decreasing

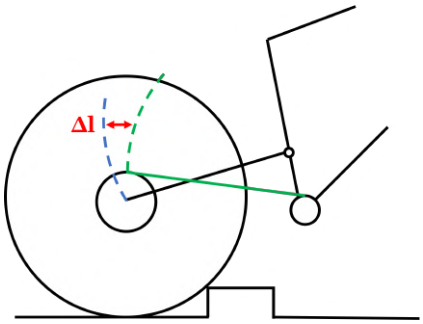

Figure 5: Pedal Kickback

ratio towards the end of the travel to handle intense shocks without bottoming out prematurely. The rear suspension's shock absorption results from the relationship between the rear suspension's leverage ratio and the spring-damper element's characteristic. Air chamber-based elements show progression, while coil springs offer linear behavior. Coil springs have a lower initial breakaway force, but air springs, needing extra seals, have higher friction. A progressive kinematics setup allows for the use of a steel coil.

The goal was to develop a kinematic that relies on a high pivot point and a progressive leverage ratio, enabling effective obstacle absorption in the SAG range and impact protection toward the travel's end. Due to a progressive layout the design should allow using a steel coil with low breakaway force. Targeting 100% anti-squat in the SAG range should optimize pedaling efficiency. Anti-rise values, less consensual in the industry, hold lower priority. The developed mechanism was optimized using "Kinematrix" software, designed to optimize kinematic systems according to predefined conditions and desired specifications. The alignment of the kinematics constituted an iterative process, accompanied by optimization from a CAD design to assess the constructive implementation.

2.3. Materials

According to the developed concept, tapered steel tubes are intended for the construction of the main frame. These tubes are specially produced for bicycle construction in terms of geometry and material properties, with two major manufacturers in Europe. Due to limited data on tube materials and delivery conditions, a series of experiments was conducted. The aim of this investigation was to evaluate the ideal material for the planned joining processes and to estimate the softening due to heat influence. The materials tested share the manufacturer's claim of good weldability and do not require post-weld heat treatment. Therefore, the preliminary study focuses solely on assessing softening during the brazing process. For the investigations, the following tubes were selected:

- Columbus: Zona (tempered steel) / XCR (stainless steel)
- Reynolds: 853 (tempered steel) / 931 (stainless steel)

From the tubes, 20 mm segments were extracted for testing, taken from the thin-walled section with a 0.5 mm thickness. These samples were then subjected to heat treatment matching the parameters of the brazing system. The heat treatment was done in a nitrogen atmosphere, followed by slow cooling in air. Vickers hardness testing was then performed on samples of each tube material in four conditions (2 / 5 / 10 minutes at 730°C & initial condition), with three measurements taken per sample at the core of the tube segment for calculating the average.

The evaluation of materials for turning and milling parts was based on manufacturing and mechanical requirements.

The 3D-printed components are made from 17-4 PH stainless steel, known for its excellent mechanical properties and high ductility. Additionally, this steel is corrosion-resistant and exhibits sufficient weldability.

2.4. Joining Processes

The studies about the joining processes serve as the foundation for frame construction, involving a practical test series for brazing and welding joints in combination with 3D-printed components. The aim is to ensure the feasibility of the assembly concept and ultimately refine the constructive implementation.

To assess the strength of the brazed joint, test samples were fabricated, brazed, and subsequently sheared using a tensile testing machine. The shear test aims to estimate the shear strength of the brazing system.

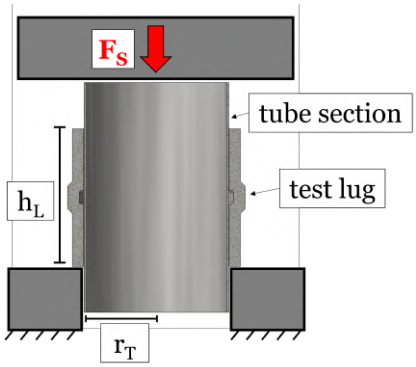

Figure 6: Shear Test

$$\tau = \frac{F_S}{A} \tag{3}$$

$$A = r_T \cdot 2\pi \cdot h_L \tag{4}$$

In addition to the shear test, another series of test samples were prepared for metallurgical analysis of the brazed joint. For the evaluation of the brazed joint, metallurgical cross-sections were prepared. Initially, the test specimens were cut in half radially using a cutoff wheel. The halved specimens were embedded to prevent damage to the brazed joint during subsequent cutting steps. Another cut was made axially. The specimens were embedded again, followed by grinding and polishing. The brazed joint was then examined and measured using a light microscope. During the evaluation, the gap width and the length of the area without filler metal were measured per joint. The

brazed gap width is reported as the average of three measurements. The metallurgical analysis of the brazed joint is shown in the following figure 7.

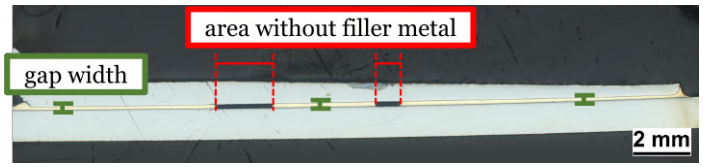

Figure 7: Metallurgical analysis of brazing joints

Compared to brazing, welding benefits from better documented processes. Material datasheets indicate sufficient to good weldability for the joining partners. Reynolds has successfully utilized welded joints between 3D-printed components and Reynolds 931 steel tubes in previous frame constructions. Thus, the welding evaluation focused on assessing the process, partner, and the visual and metallurgical quality of the joint.

For the initial assessment of the welding joint, several 3D-printed test specimens were fabricated and welded to tube segments using different methods. An evaluation followed, focusing on the visual and metallurgical quality. Metallurgical cross-sections were prepared to evaluate welding quality, while hardness measurements of various microstructural zones provided an estimation of mechanical properties. The test series included the following methods:

- TIG welding without filler metal, manual
- TIG welding with filler metal, manual
- Laser welding with filler metal, automated

After welding, visual inspections of the welds were conducted. Subsequently, sample segments were extracted, embedded, ground, and polished. Etching was performed using an appropriate etchant for martensitic stainless steels, followed by microstructure examination using a light microscope. Vickers hardness measurements were then conducted in various microstructural zones, with three measurements taken per zone and averaged.

2.5. Design and Dimensioning

In the initial phase, bearing layout and preliminary sizing of the frame tubes were conducted. These aspects determine the available space for topology optimization and serve as the basis for designing the respective components. Following the determination of bearing and tube dimensions, topology optimization by submodell method of the 3D-printed parts and the swing arm was performed. Finally, the overall model is assessed in all load cases using finite element analysis.

The design is based on the testing protocol established by EFBE for the category of downhill/freeride bicycles (Category 5). This testing program consists of eight consecutive strength tests of the frame structure. These tests include cyclic loading scenarios, as well as assessments for maximum and overload conditions, considering a system weight of 120 kg.

For topology optimization, a structural FEA of the full model is initially performed under specific load cases. Subsequently, these results are applied to a submodel, representing a section of the full model, focusing on the component undergoing optimization. The displacements from the full model serve as boundary conditions for the submodel's FEA, facilitating topology optimization. This method allows for efficient computation of the complex full model with coarse meshing, while enabling finer meshing of the submodel. The topology optimization serves as a guide for material placement to achieve maximum stiffness. While stress analysis on the component is pending, the remodeled part is integrated back into the submodel for strength evaluation under specific loading conditions. The optimization process is illustrated on figure 8.

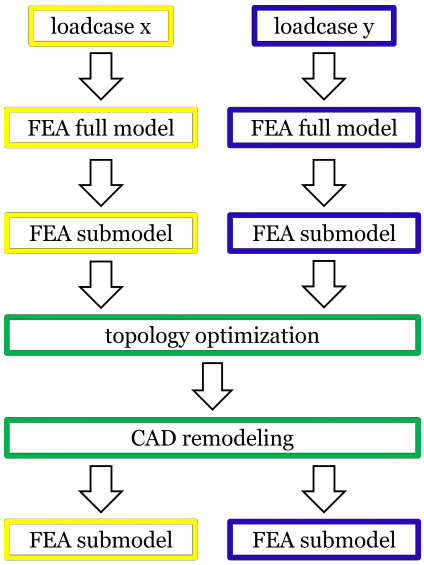

Figure 8: topology optimization process

Following the topology optimization and construction of individual components, a FEA of the final model was carried out throughout the entire testing program. Since the testing program applies cyclic and static load cases sequentially to a frame, the simulation results undergo linear damage accumulation according to the Miner's rule [1, p. 158].

$$\sum_i \frac{N_i}{N_{Bi}} = 1 \tag{5}$$

The tolerable cycles are estimated using the Goodman method [1, p. 157].

$$\Delta\sigma_{\sigma_M} = \Delta\sigma_{\sigma_0} \times (1 - \frac{\sigma_M}{R_m}) \tag{6}$$

The results of the static load cases are assessed based on the yield strength.

3. Results

3.1. Frame Geometry

The frame geometry for the prototype is aimed at an enduro bike with a focus on downhill riding, while still providing comfortable handling. The frame design aims to strike a sensible compromise between these attributes, serving as a neutral basis for initial experiences.

Prototype Geometry	
Wheelbase	1272 mm
Stack	635 mm
Reach	480 mm
Seat tube angle	77.5°
Bottom bracket height	345 mm
Chain stay	445 mm
Head tube angle	64°

Table 1: Prototype Geometry

3.2. Kinematics

Based on a comprehensive brainstorming session, various suspension linkage concepts were generated and evaluated. The chosen design offers considerable design freedom regarding the leverage ratio and enables high progression. Additionally, a preliminary study demonstrated that the arrangement of necessary components can be constructed sensibly.

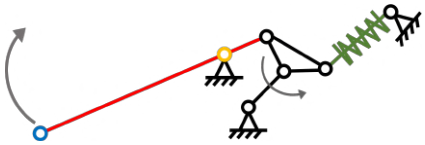

Figure 9: kinematic mechanism

The resulting kinematic characteristics of the suspension are depicted in the following graphics.

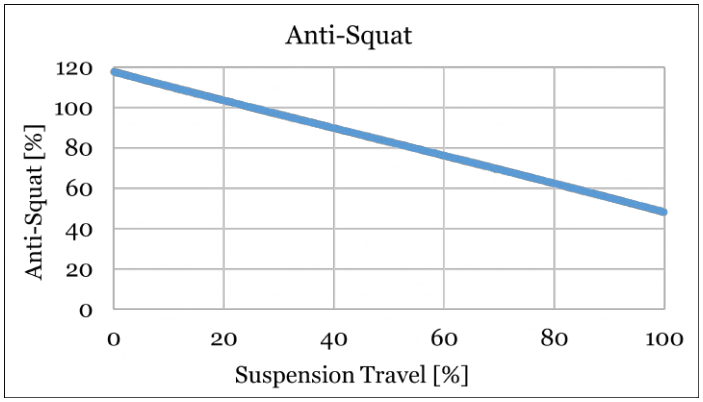

Figure 10: Anti-Squat

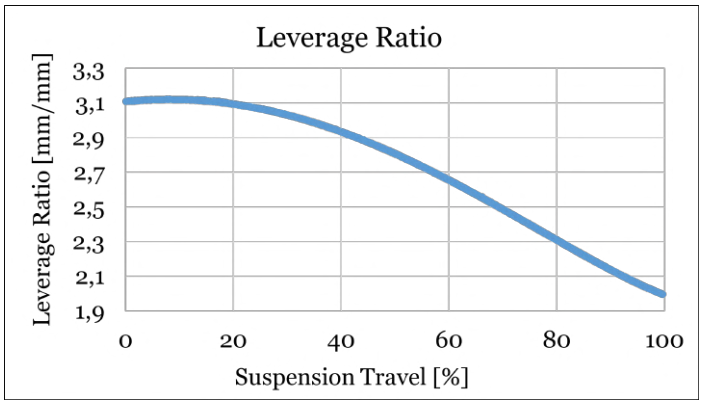

Figure 11: Leverage Ratio

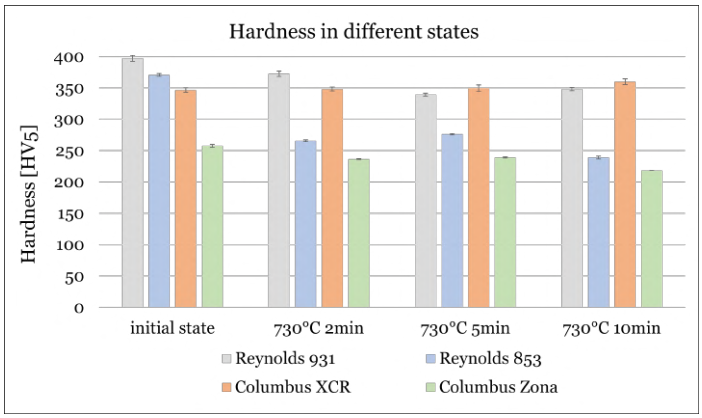

Figure 12: hardness of tube material after annealing experiments

3.3. Materials

The hardness measurements of various heat treatment conditions from the conducted annealing experiments of the steel tubes are illustrated in the graph on figure 12.

The evaluation of materials for turning and milling components yielded the following results. The axles are crafted from EN AW-7075 T6 aluminum alloy. This alloy is popular for its high strength and commonly used in aerospace. The swingarm employs an EN AW-2099-T83 alloy, known as an aluminum-lithium (Al-Li) alloy, prized for its superior strength-to-weight ratio and weldability. Compared to other aluminum alloys, this material offers approximately a 10% higher modulus of elasticity with a 3% lower density. The mechanically less stressed components are fabricated from EN AW-6082 T6.

3.4. Joining Processes

The shear strength measurement data from the braze connections are presented in the following table.

shear strength	
average shear strength	126 MPa
standard deviation	55 MPa

Table 2: shear strength measurement results

Figure 13 illustrates the percentage of area without filler metal in the braze joint in function of the gap width.

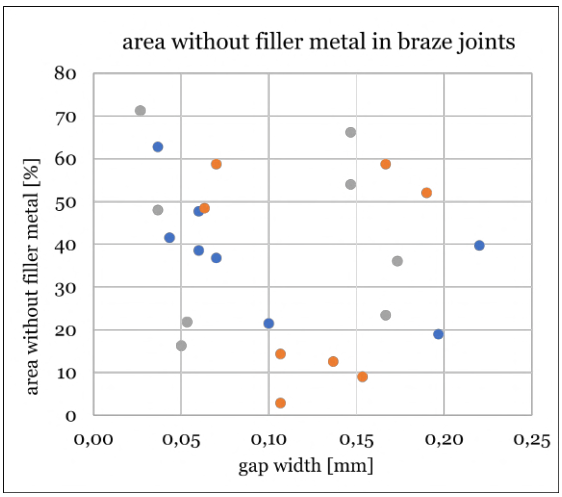

Figure 13: area without filler metal in braze joints

The following figure 14 depict the optical quality of the welds, as well as a microscopic image of the produced micrographs.

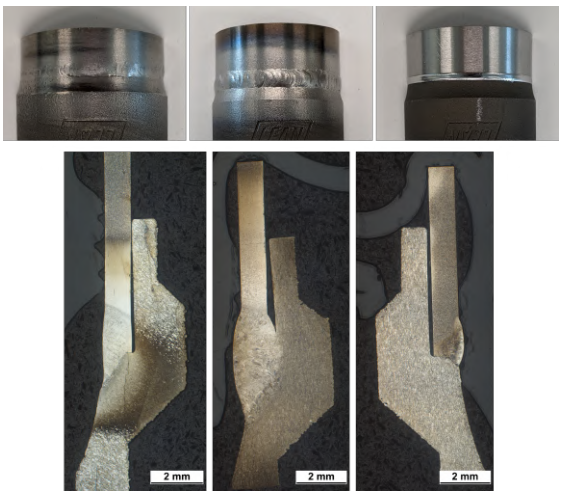

Figure 14: optical and metallurgical results for weld joints

The hardness measurements yielded the following results. The hardness in the tube area is slightly higher at 353 HV1 compared to the weld seam hardness of 345 HV1. In contrast, the lowest hardness is observed in the lug area at 325 HV1.

3.5. Design and Dimensioning

The results of the topology optimization and the remodeled body are exemplified in Figure 15.

In the following, the results from the simulations are presented. Concerning the cyclic loads, the critical areas of each component were analyzed and compiled. The safety factor against fatigue and the resulting damage value were calculated. The static load cases depict the utilization factor of the yield

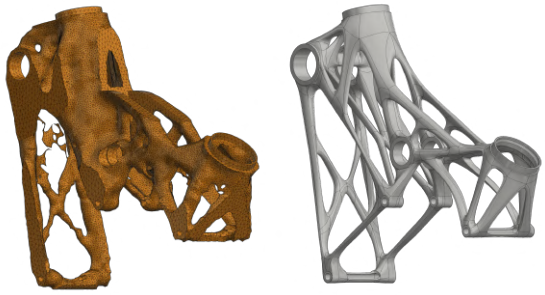

Figure 15: results of topology optimization

strength, where the color red corresponds to a factor of 1 and above.

Figure 16 shows the most critical parts with the corresponding damage values summed over all cyclic load cases.

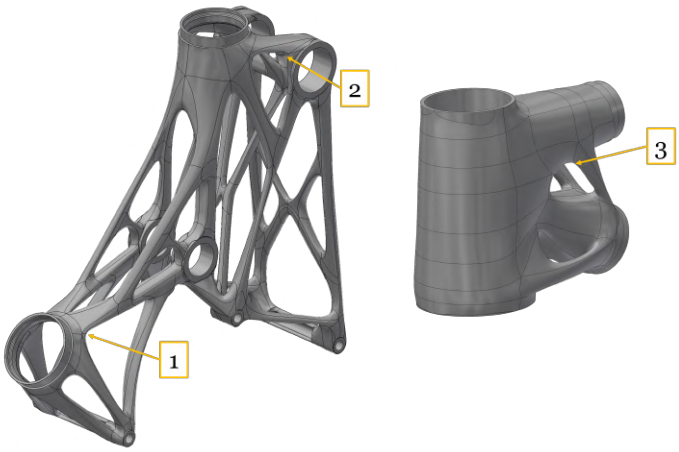

Figure 16: critical areas due to cyclic loads

area	damage value
1	0.8
2	0.7
3	0.8

Table 3: summed damage values in critical areas

The effect of static load cases on the structure is demonstrated through the figures in the appendix. The utilization factor of the swingarm and 3D-printed components ranges up to 1.3 depending on the area.

4. Discussion

The conducted process for evaluating the frame geometry does not represent an analytical method but rather served as an approach to understand the effects of individual geometry elements on practical driving behavior and to gain insights for prototype geometry.

The anti-rise value in the SAG range is approximately 135%. Despite some disagreement within the bicycle industry regarding its significance, it's accepted as it mirrors only an idealized

state of rear-wheel braking. For systems with a high pivot point, a high anti-rise leads to suspension compression during braking. The anti-squat value now stands precisely at 100% in the SAG range, indicating that chain force counters mass transfer, achieving moment equilibrium during acceleration. Leverage ratio tuning prioritized a high ratio at the start of suspension travel for absorbing small to medium obstacles, with a decrease towards the end to prevent bottoming out under heavy loads. While the kinematic design methodology relies on simplifications and assumptions, it's a well-established practice in the bicycle industry. Prototyping allows real-world testing to validate the tuning performed.

Utilizing the minimum measured value obtained from the shear tests for the shear strength of the solder joint, it necessitates an overlap length exceeding 17 mm for the joint to fail after the tubing. From a structural perspective, satisfying this criterion presents no challenges. TIG welding with filler material provides adequate quality and simplicity compared to laser welding, which would require frequent repositioning and realignment during prototype fabrication. For a single-frame production, this would be impractical. Additionally, both laser and TIG welding without filler material would necessitate further parameter studies for sufficient weld depth and strength. Therefore, the prototype is welded using the TIG process with filler material. Hardness measurements show minimal softening of the structure, indicating no embrittlement of the weld seams.

In the design process, it's essential to consider that the lifespan calculations are primarily estimations. Additionally, 3D-printed components introduce quality variations, and surface quality significantly influences cyclic properties. For these reasons, Lean Cycles will extensively test the frame. Furthermore, strain gauge measurements are planned to determine operational loads and validate simulations thoroughly. These measurements will also help assess the relationship between the considered load cases and riding on challenging terrain.

5. Summary and conclusions

The concept phase was followed by defining an appropriate frame geometry. Key geometry elements were depicted and described, followed by test rides to evaluate the prototype. The resulting geometry was tailored to serve as a neutral base for an enduro bike.

The kinematic development utilized a quasi-static approach, common in bicycle manufacturing despite its simplifications. It involved deriving and describing key parameters such as anti-squat, anti-rise, wheel path, and leverage ratio. Through intensive brainstorming, different suspension linkage concepts were generated and assessed. The selected variant allows for considerable design freedom regarding the leverage ratio. Utilizing the "Kinematrix" software for the optimization, an iterative process was conducted to meet specified requirements. This process was complemented by the construction of a 3D model to address design conflicts, resulting in a solution that met the desired goals of a progressive leverage ratio combined with an efficient suspension.

Prior to construction, materials were evaluated. Reynolds 931 steel was chosen for frame tubes due to minimal softening during brazing and suitability for welding. The swingarm is made from an Al-Li alloy, offering a 10% higher modulus of elasticity and 3% lower density compared to other aluminum alloys, with good weldability. 3D printed components are made from 17-4 PH steel, known for its excellent mechanical properties, high ductility, corrosion resistance, and weldability.

Various preliminary studies were conducted to assess the feasibility of the assembly concept for frame construction. Application-oriented test series were carried out for brazing and welding joints, along with 3D printed components. The experiments demonstrated that brazed joints exhibited sufficient mechanical properties even with small overlap. TIG welding with filler provided adequate optical quality and was the simplest method, with metallurgical analysis confirming weld strength close to the base material and no embrittlement.

Load cases for the overall design are based on EFBE testing institute standards. The test program applies six cyclic and two static load cases sequentially to a frame. The available space for topology optimization was determined by defining bearing dimensions using multibody simulations. Finite element simulations estimated tube dimensions. Topology optimization of main components was conducted via the submodel method, followed by remodelling based on optimization results. Structural mechanics calculations for the entire test program were performed using the final model geometry. Linear damage accumulation was applied using the Miner rule for cyclic load cases, with cycle limits estimated following Goodman's criteria. Static load case results were assessed based on yield strength. The structure was found to offer sufficient strength for category 5 downhill segments.

Acknowledgements

I extend my sincere gratitude to everyone who contributed to this project. Special thanks to my advisor, Prof. Dr. Arne Wahlen, for his invaluable guidance and support throughout. I am grateful for the collaborative efforts and insights provided by my colleagues, mentors, and partners, which significantly enriched this work.

References

[1] Ashby, M., Jones, D., 2006. Werkstoffe 1: Eigenschaften, Mechanismen und Anwendungen: Deutsche Ausgabe herausgegeben von Michael Heinzelmann. Spektrum Akademischer Verlag.

[2] Dr.-Ing. Markus Hiebel, J.N., 2016. Technische, ökonomische und gesellschaftliche faktoren von stahlschrott. Fraunhofer-Institut für Umwelt-, Sicherheits- und Energietechnik .

[3] Good, C., McPhee, J., 1999. Dynamics of mountain bicycles with rear suspensions:modelling and simulation. Sports Engineering .

[4] Gross, E., 1997. Betriebslastenermittlung, Dimensionierung, strukturmechanische und fahrwerkstechnische Untersuchungen von Mountainbikes. Fortschritt-Berichte VDI. Reihe 12. Verkehrstechnik/Fahrzeugtechnik, VDI-Verlag.

[5] J., E.R..K., 2014. Kohlenstofffasern wiedergewinnen. Kunststoffe, Bd. 6 .

[6] Macherauch, E., Zoch, H.W., 2011. Risszähigkeit. Vieweg und Teubner, Wiesbaden. pp. 320–330.

[7] Menges, G., 2011. Werkstoffkunde der Kunststoffe. volume 2620. Walter de Gruyter.
[8] Schürmann, H., 2007. Konstruieren Mit Faser-Kunststoff-Verbunden. VDI-Buch, Springer Berlin Heidelberg.
[9] Susanne Böhler, Dr. Wolfgang Irrek, D.K.K.D.M.K.D.R., 2008. Zukunftsfähiges Deutschland in einer globalisierten Welt ein Anstoss zur gesellschaftlichen Debatte: eine Studie des Wuppertal Instituts für Klima, Umwelt, Energie. Fischer Taschenbuch Verlag, Frankfurt am Main.
[10] T.E. Norgate, S. Jahanshahi, W.R., 2006. Assessing the environmental impact of metal production processes. Journal of Cleaner Production .

Appendix A. Stresses due to static load cases

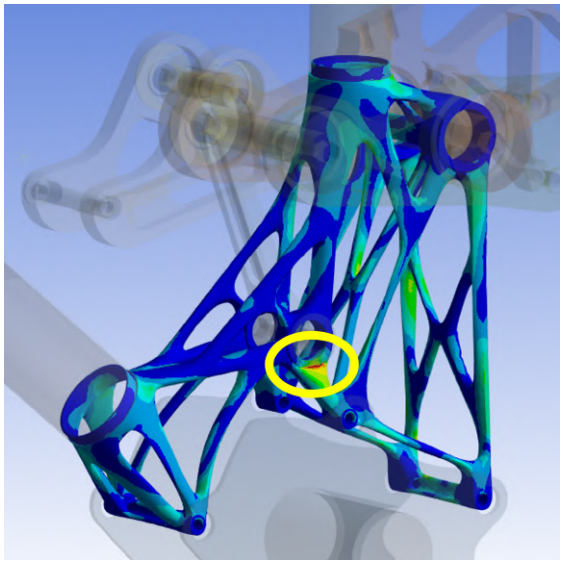

Figure A.17: utilization factor: 1.3

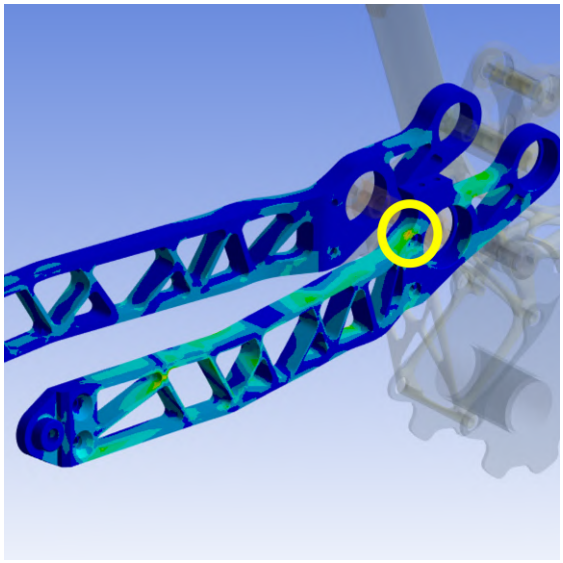

Figure A.18: utilization factor: 1